APL Materials

RESEARCH ARTICLE | MAY 01 2023

Experiment on terahertz metasurfaces of metal split ring resonators with bound state in the continuum

Tailin Zhang; Xingyuan Zhang; Yun Shen ✉; ... et. al

Check for updates

APL Mater 11, 051102 (2023)
https://doi.org/10.1063/5.0147843

View Online
Export Citation
CrossMark

Downloaded from http://pubs.aip.org/aip/apm/article-pdf/doi/10.1063/5.0147843/17167793/051102_1_5.0147843.pdf

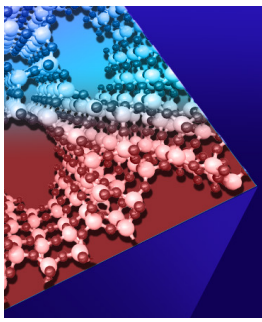
APL Materials
Special Topic:
Open Framework Materials
Submit Today!
AIP Publishing

AIP Publishing

Experiment on terahertz metasurfaces of metal split ring resonators with bound state in the continuum

Cite as: APL Mater. 11, 051102 (2023); doi: 10.1063/5.0147843
Submitted: 27 February 2023 • Accepted: 10 April 2023 •
Published Online: 1 May 2023

View Online Export Citation CrossMark

Tailin Zhang,[1] Xingyuan Zhang,[2] Yun Shen,[1,3,a)] Yinsheng Xu,[1] Laibin Luo,[1] Jianqiang Gu,[2,a)] Sijia Yang,[3] Jie Xu,[4] and Xiaohua Deng[2]

AFFILIATIONS

[1] Department of Physics, School of Physics and Materials Science, Nanchang University, Nanchang 330031, China
[2] Center for Terahertz Waves and College of Precision Instrument and Optoelectronics Engineering, Tianjin University, Tianjin 300072, China
[3] Institute of Space Science and Technology, Nanchang University, Nanchang 330031, China
[4] School of Medical Information and Engineering, Southwest Medical University, Luzhou 646000, China

[a)] **Authors to whom correspondence should be addressed:** shenyun@ncu.edu.cn and gjq@tju.edu.cn

ABSTRACT

A bound state in the continuum (BIC) is a wave that coexists with a continuous wave but remains localized. In the terahertz band, BIC can design devices with an ultra-high mass factor (Q factor), which is of great value for terahertz science and technology, so we designed a terahertz BIC metasurface structure composed of metal split ring resonators (SRRs). According to the symmetric protection principle of superlattice mode, the leakage process of BIC states to the far field is studied by changing the gap width of SRR. By introducing multiple SRRs and changing their arrangement, we obtain three superlattice modes and BIC states. The leakage of BIC states into the far field is observed experimentally, which means that observable quasi-BIC patterns are formed. We verify a feasible method that allows for flexible design and implementation of BIC.

© 2023 Author(s). All article content, except where otherwise noted, is licensed under a Creative Commons Attribution (CC BY) license (http://creativecommons.org/licenses/by/4.0/). https://doi.org/10.1063/5.0147843

I. INTRODUCTION

High-quality factor (high-Q) optical resonators have attracted much attention due to their rich physical phenomena and potential applications in enhanced light emission,[1] chemical and biological sensing,[2,3] non-linear optics, etc.[4] However, the reported Q values of terahertz devices are mostly in the order of 10, which cannot meet the practical requirements of applications.[5,6] Bound state in the continuum (BIC) refers to the trapped state in the radiation continuum of a system, enabling an infinitely high-quality factor and a correspondingly infinite lifetime of the resonance.[7–9] The emergence of BIC provides unprecedented possibilities for the realization of terahertz functional devices with an ultra-high Q factor.[10–12] Among them, BICs were mainly realized by three methods: structural symmetry protection, destructive interference between resonators, and inverse construction.[13,14] So far, BICs have been achieved in coupled waveguides, gratings, photonic crystals, photonic circuits, metamaterials/metasurfaces, and so on.[15–20] Particularly, because of the high freedom level in the design of the metasurfaces, the demonstration of BICs in metasurfaces is extended to a wide spectrum from visible light to microwaves[21–23] and found in various systems including perforated dielectric plates,[24] double-gap split ring resonators,[25] semiconductor blocks,[26] and free-standing structures.[27] Actually, ideal BICs cannot be observed in the electromagnetic spectrum because of their infinite lifetime and zero leakage.[28] However, by introducing structural perturbations into the BIC metasurface, quasi-BICs (identifiable by a high-Q resonant mode induced by the coupling of two low-Q modes) emerge in the far-field response.[29] In 2022, Zhang *et al.* studied terahertz metasurface BIC composed of metal split ring resonators (SRRs) using the method of structural symmetry protection.[30] On the other hand, terahertz (THz) technology shows great potential in security imaging, wireless

Downloaded from http://pubs.aip.org/aip/apm/article-pdf/doi/10.1063/5.0147843/17167793/051102_1_5.0147843.pdf

© Author(s) 2023

communication, and fingerprint spectroscopy,[31–33] while THz functional devices with high Q factors, for example, high-sensitive sensors, narrow linewidth filters, and slow light modulators, are in high demand.[34,35] Although the reported BIC is also formed by the metal SRR, they use the translation symmetry of the SRR array to obtain the BIC. We experimentally validated the method of obtaining different BICs by arranging classical single-gap metallic rings in different configurations.

In this paper, we use the classical metal SRR as the basic unit, break through the symmetry of the SRR's structure, and combine multiple SRRs to form a new superlattice. Using CST Microwave Studio software, numerical simulation and experimental research on the SRR superlattice were carried out. By changing the gap width of adjacent SRRs, the existence of BIC states on the metal SRR metasurface is verified, and the quasi-BIC (QBIC) resonance formed by BIC leakage is obtained simultaneously. Research has shown that breaking symmetry is a reasonable way to achieve BICs on metasurfaces. The metasurface demonstrated in this paper will promote the development of high-Q THz devices, and the designed metal SRR metasurface has a precise mechanism and is easy to prepare.

II. SIMULATION

The shape and size of the metal SRR element structure designed in this paper are shown in Fig. 1(a). The specific structural parameters of the SRR are b = 8 μm, g = 12 μm, and a = 48 μm. The layer of metallic SRRs has a thickness of 200 nm and is located on the surface of a highly resistive silicon substrate. By arranging the two SRRs in different ways, two kinds of superlattices ① and ②, as shown in Figs. 1(b) and 1(c), are formed. All BIC/QBIC structures in this paper are composed of SRR units with a period of 68 μm, as shown in Fig. 1(d). Only the gap width g will change in the discussion, forming a QBIC state with perturbative symmetry. To determine the existence of BIC modes in different arrays of SRRs,

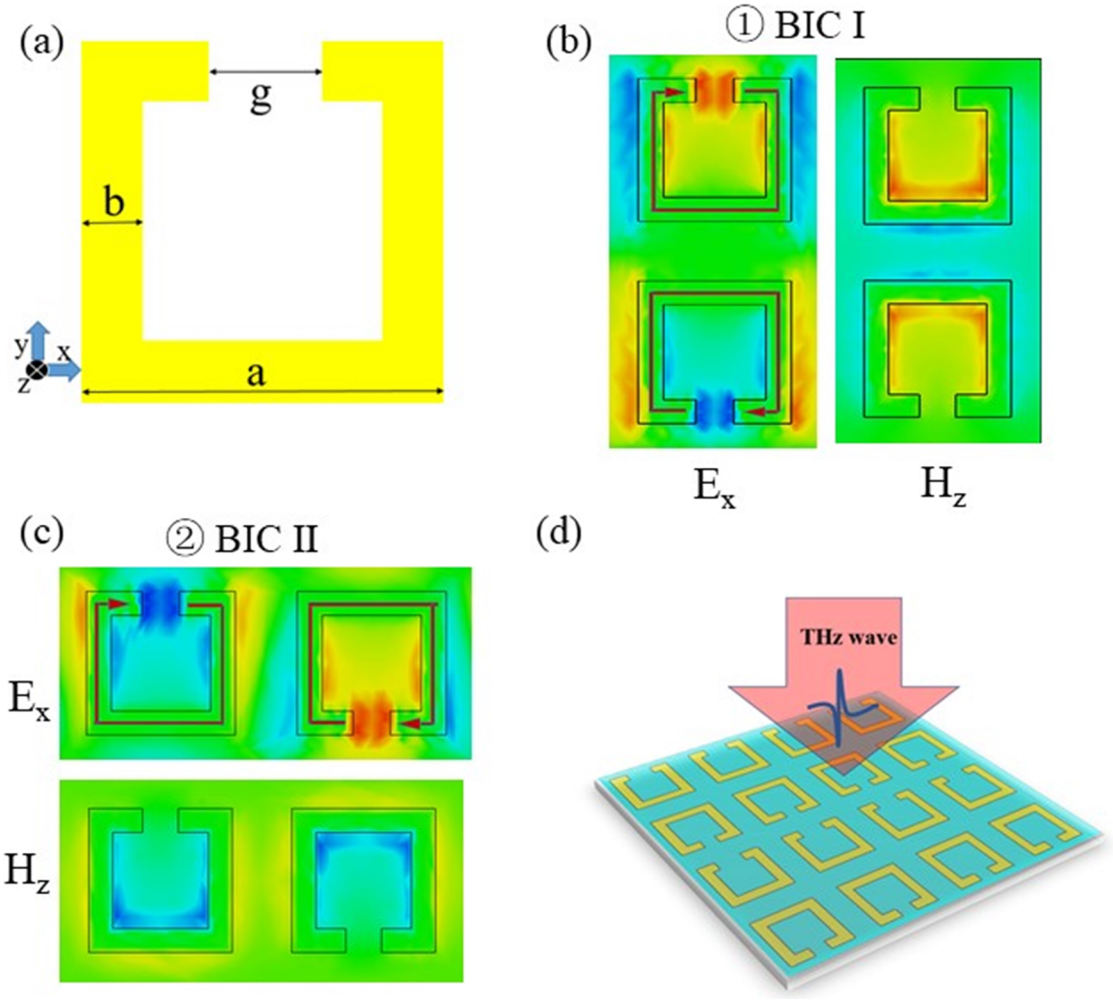

FIG. 1. (a): SRR basic dimension diagram. (b): BIC I electric field x component, current distribution and magnetic field distribution with a frequency of 0.400 THz. (c): BIC II electric field x component, current distribution and magnetic field distribution with a frequency of 0.450 THz. (d): Schematic of the metallic SRR arrays on a silicon substrate.

Downloaded from http://pubs.aip.org/aip/apm/article-pdf/doi/10.1063/5.0147843/17167793/051102_1_5.0147843.pdf

© Author(s) 2023

we used the eigenmode solver in the CST Microwave Studio software to calculate the eigenmodes of superlattices ① and ②. Among them, the boundary conditions of x and y are electric walls ($E_t = 0$), and the boundary conditions of z are open added space. In the calculation, phases x and y were set to 0, corresponding to the mode of the Γ point in the calculation energy band. The metal material was set as a perfect electrical conductor (PEC) to eliminate the influence of ohmic losses, and the substrate was considered non-absorbing silicon. The simulation results are shown in Figs. 1(b) and 1(c), where the superlattices ① and ② form their respective bound states

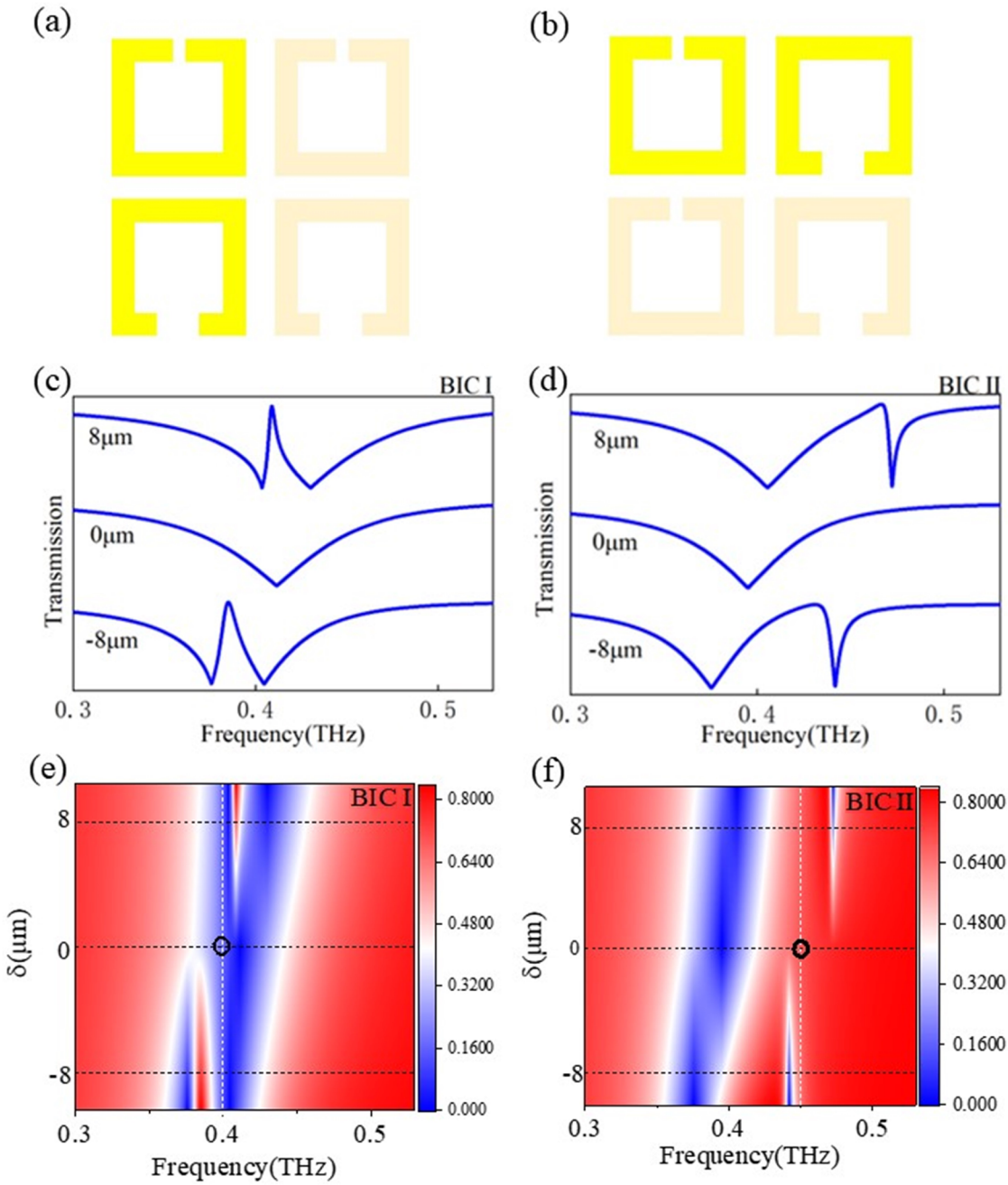

FIG. 2. (a) and (b): Schematic diagrams of the superlattices ① and ② after breaking the structural symmetry. (c) and (d): For the superlattices ① and ②, the transmission spectra of three different cases of $\delta = -8$, 0, and 8 μm. (e) and (f): Corresponding to BIC I and BIC II, respectively, the pseudo-color map of the transmission spectrum after changing the asymmetry.

Downloaded from http://pubs.aip.org/aip/apm/article-pdf/doi/10.1063/5.0147843/17167793/051102_1_5.0147843.pdf

© Author(s) 2023

at 0.400 and 0.450 THz, respectively. Since the Γ point corresponds to the perpendicular incidence and is in the continuum domain, these two bound states are the BIC states, denoted as BIC I and BIC II.

The electric field amplitude distribution and current distribution on SRR shown in Figs. 1(b) and 1(c) indicate that BIC I and BIC II are based on the LC resonance of SRR, and the current distribution in SRR belongs to classical LC circulation. The electric fields of the two SRR structures in the superlattice are antisymmetric. The magnetic field distributions of BIC I and BIC II are shown in Figs. 1(b) and 1(c).

BIC has an infinitely narrow linewidth, which is higher than the frequency resolution of all systems and cannot be directly observed in the spectrum, so most of the reported works have indirectly verified the existence of BIC by introducing perturbations and observing the process of BIC transformation into QBIC. As shown in Figs. 2(a) and 2(b), this paper introduces structural perturbation by modifying the gap of one SRR in the superlattice (upper SRR for superlattice ① and left SRR for superlattice ②) to break the symmetry of the superlattice. The leakage caused by perturbation BIC was simulated by using the frequency-domain solver in the CST Microwave Studio software, where the material model was consistent with the characteristic mode calculation. The boundary condition of x and y was set as a unit cell, and the boundary condition of z was set as an open added space. The frequency range of the simulation was set to 0.300–0.600 THz, and the simulation results are shown in Figs. 2(c) and 2(d). We denote the change in structure as $\delta = g - 12$ (μm), where the gap g takes the values of 20, 12, and 4 μm. It can be seen from the figures that when $\delta = 0$ μm, there is no narrow-linewidth resonance in the transmission spectrum of the metasurface composed of superlattices ① and ② at 0.400 and 0.450 THz calculated by the eigenmode and instead a wide LC resonance of SRR. However, when $\delta \neq 0$ μm, asymmetric Fano linear resonance will appear near 0.400 and 0.450 THz. The asymmetric Fano linear resonance for superlattice ① [Fig. 2(c)] is formed by the coupling of QBIC resonance and LC resonance.

The superlattice ② [Fig. 2(d)] is formed by coupling the QBIC resonance and the non-resonant continuum domain transmission of the SRR. The sign of δ determines whether the frequency of the Fano resonance is higher or lower than the BIC frequency. |δ|

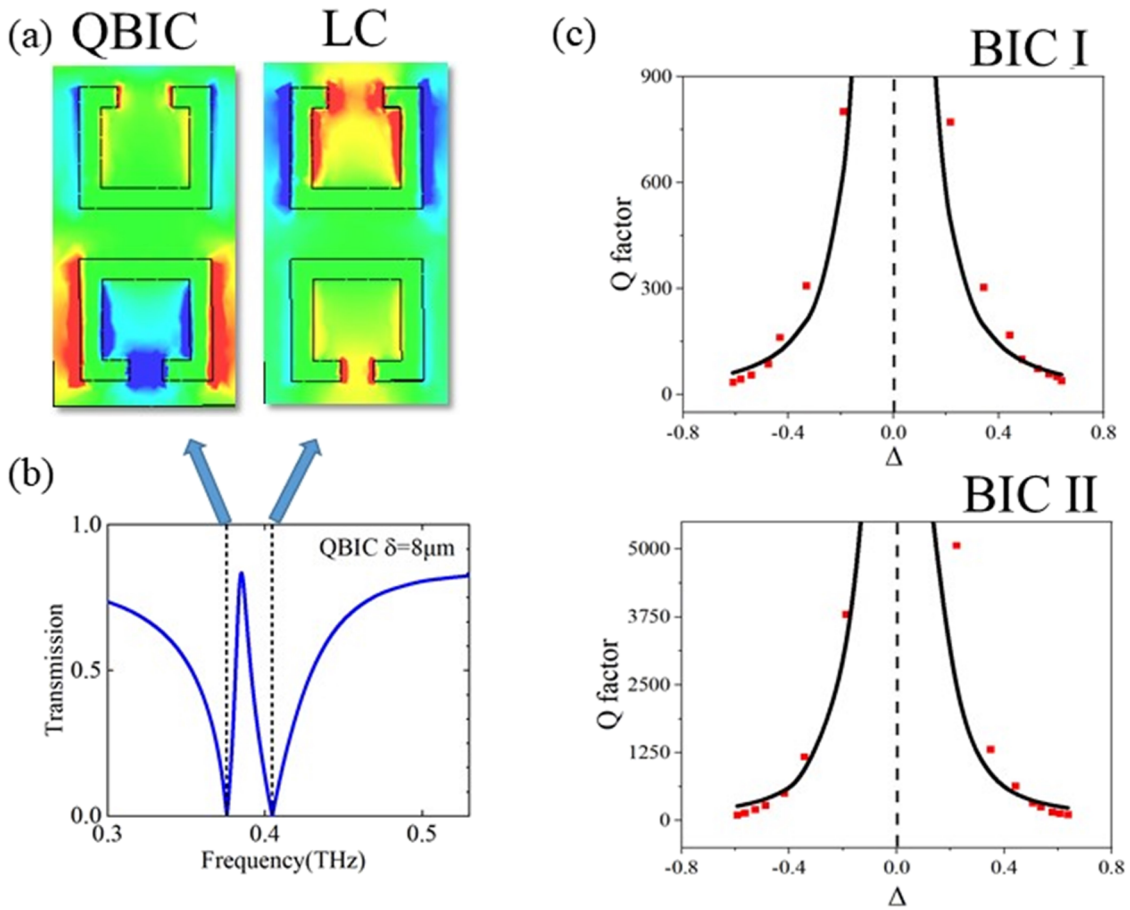

FIG. 3. (a): Distribution of the x-component of the electric field for two different resonances. (b): Transmission spectrum of superlattice ① with $\delta = -8$ μm. (c): Variation of Q value with a degree of asymmetry.

Downloaded from http://pubs.aip.org/aip/apm/article-pdf/doi/10.1063/5.0147843/17167793/051102_1_5.0147843.pdf

© Author(s) 2023

determines the width of the Fano resonance line. The pseudo-color diagram is shown in Figs. 2(e) and 2(f), where the vertical axis is the asymmetry δ of SRR structure, the horizontal axis is frequency, the vertical dashed line indicates the frequency value of BIC calculated by simulation, the small circle indicates the position of BIC, and the horizontal dashed line indicates the section position corresponding to the transmission spectrum in Figs. 2(c) and 2(d). Pseudo-color brightness represents the amplitude of the transmission spectrum at each δ. With the change of δ from negative to positive, the frequency of Fano resonant disappearance is exactly 0.400 and 0.450 THz. This BIC state is in perfect agreement with the reported BIC verification method, which proves the existence of BIC I and BIC II.

According to Koshelev *et al.*,[36] the QBIC resonances that appear when $\delta \neq 0$ μm originate from the far-field leakage formed by the antiphase resonances of the adjacent SRRs after the symmetry break and can no longer fully interfere with the cancellation. Take the Fano resonance at $\delta = 8$ μm in the superlattice ① as an example; as shown in Fig. 3(b), two resonant valleys appear in the transmission spectrum, and the low-frequency resonant valley with a narrow linewidth is derived from QBIC resonance. It can be seen that the

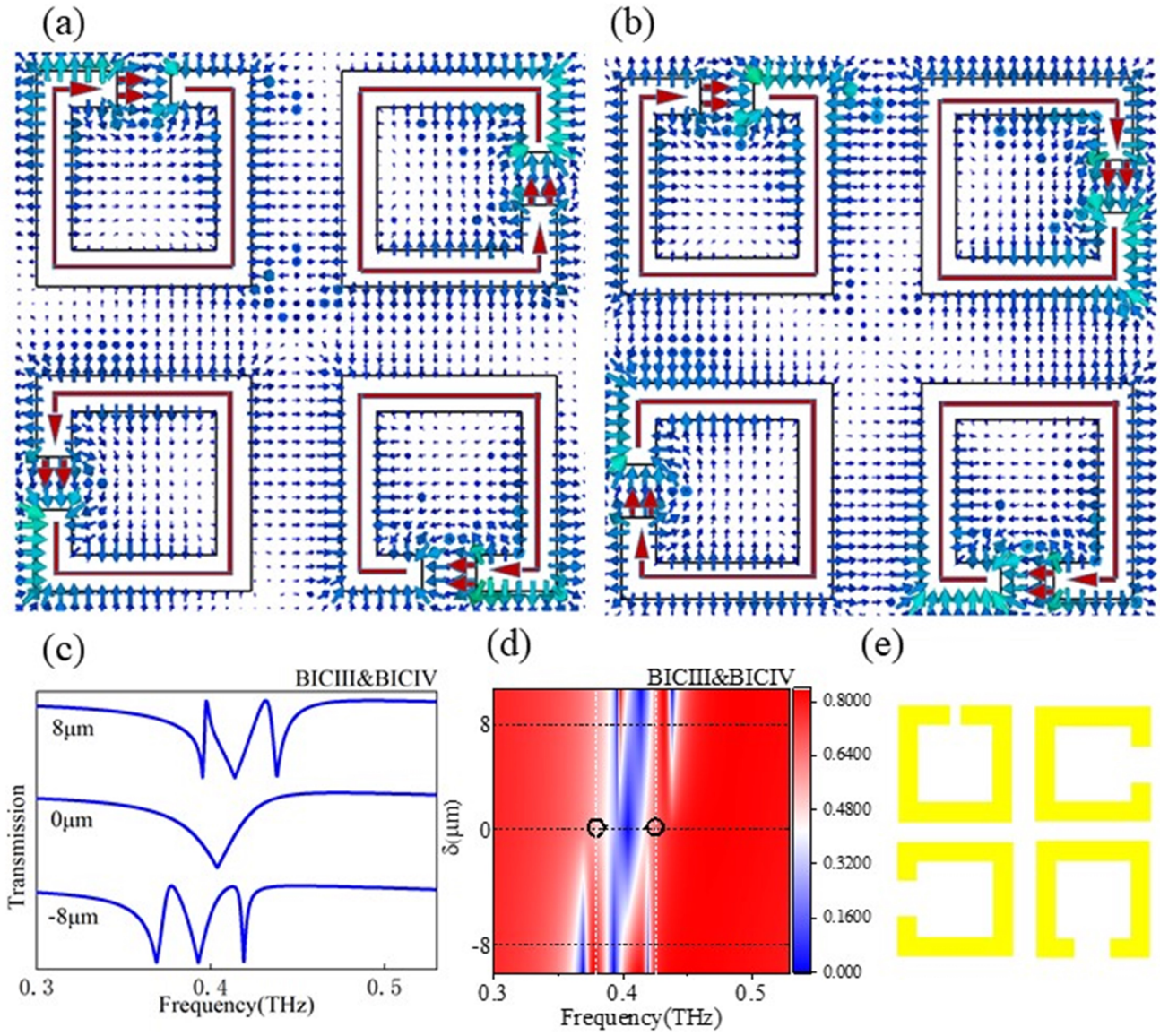

FIG. 4. (a): Electric field distribution of BIC at 0.380 THz (b): Electric field distribution of BIC at 0.425 THz. (c): Transmission spectrum after symmetry breaking of BIC structure. (d): Pseudo-color map of the transmission spectrum (e): Schematic diagram of superlattice ③ after symmetry breaking.

Downloaded from http://pubs.aip.org/aip/apm/article-pdf/doi/10.1063/5.0147843/17167793/051102_1_5.0147843.pdf

© Author(s) 2023

QBIC field distribution [Fig. 3(a)] is similar to the antisymmetric field distribution of BIC I in Fig. 1(c).

Since the resonant frequency and radiation loss of the two SRRS are no longer the same, the far-field radiation is no longer completely cancelable. The larger the difference between the gap of adjacent SRRs, the more the radiation leakage, the lower the Q value of the QBIC mode and the Fano resonance formed by its coupling. In the work of Koshelev, it was proposed that there is a quadratic inverse relationship between the Q value of QBIC and the degree of asymmetry of the structure. We can use the Fano formula to fit the simulation results,[37,38]

$$T = t_0 \cdot \left[a_1 + ia_2 + \frac{b}{\omega - \omega_0 + i\gamma} \right]^2, \quad (1)$$

where a_1 and a_2 are real numbers, representing the background radiation; b represents the resonance intensity of the Fano resonance; ω_0 represents the frequency of the Fano resonance; and γ represents the total loss of the Fano resonance. According to formula,

$$Q = \frac{\omega_0}{2\gamma}, \quad (2)$$

the Q values of Fano resonance under different degrees of asymmetry can be obtained. In addition, we plot the resulting values as a graph [Fig. 3(c)], where the x-axis is

$$\Delta = \delta/12. \quad (3)$$

For the QBIC resonance formed by superlattices ① and ②, the relationship between the Q value and the asymmetry is in good agreement with the inverse quadratic function.

Obviously, by introducing more SRR, more arrangements are allowed. Therefore, the method proposed in this paper to form a superlattice by arranging SRR provides a way to design SRR-based BIC and QBIC metasurfaces. The following is a simple illustration of the extensibility of this method by taking four SRR combinations as an example. The superlattice ③ shown in Fig. 4(a) consists of four SRRs whose opening directions are rotated clockwise in turn. Using the eigenmode solver of the CST Microwave Studio, it is calculated that two BIC states formed by LC resonant interferences of different SRRs exist in the superlattice at vertical incidence (Γ point); the frequencies are 0.380 and 0.425 THz, respectively, and are denoted as BIC III and BIC IV. The BIC electric field distribution of the superlattice ③ is shown in Figs. 4(a) and 4(b). Interestingly, as more SRRs are added, there are more ways in which the LC resonance between SRRs cancels each other out. Although BIC III and BIC IV have different electric field distributions, they are both based

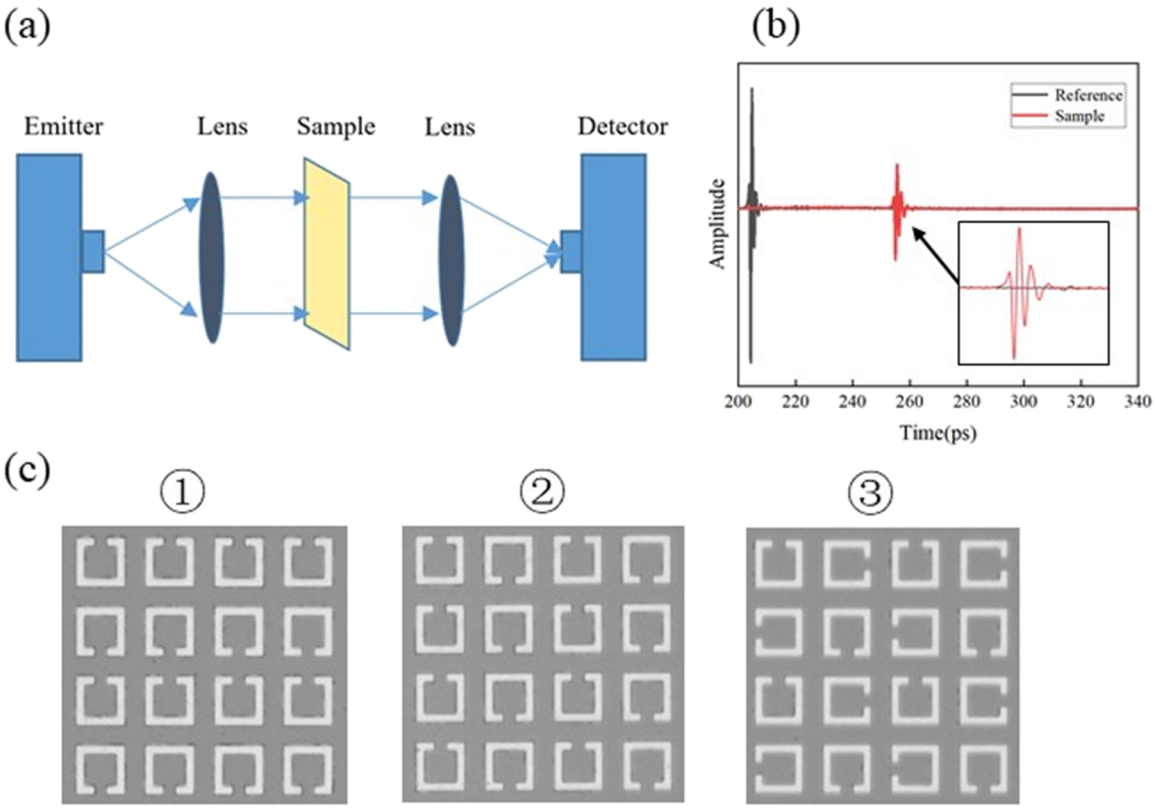

FIG. 5. (a): Schematic diagram of THz time-domain spectroscopy. (b): Time domain signal plot. (c): Micrographs of three BIC structures.

Downloaded from http://pubs.aip.org/aip/apm/article-pdf/doi/10.1063/5.0147843/17167793/051102_1_5.0147843.pdf

© Author(s) 2023

on the LC resonance of the SRR and form an antisymmetric electric field distribution. Like the previous two superlattices, the frequency domain solver of the CST Microwave Studio is still used here to verify the existence of these two BIC states numerically. By changing the gap width of the top-left SRR in the superlattice, as shown in Fig. 4(e), breaking the symmetry of the structure allows the BIC state to transform into a QBIC mode and be coupled with other resonances or the transmission background to form a Fano resonance. As shown in Fig. 4(c), two different Fano resonances will appear on the transmission spectrum, originating from two QBIC resonances.

The pseudo-color map of the transmission spectrum formed with the gap change, as shown in Fig. 4(d), shows the typical evolution process from a typical BIC to a QBIC, which verifies the existence of BIC III and BIC IV. However, the Q value of the two types of QBIC in superlattice ③ is more complex. Although the analysis of this problem is beyond the scope of this study, it provides a clear direction for subsequent related research.

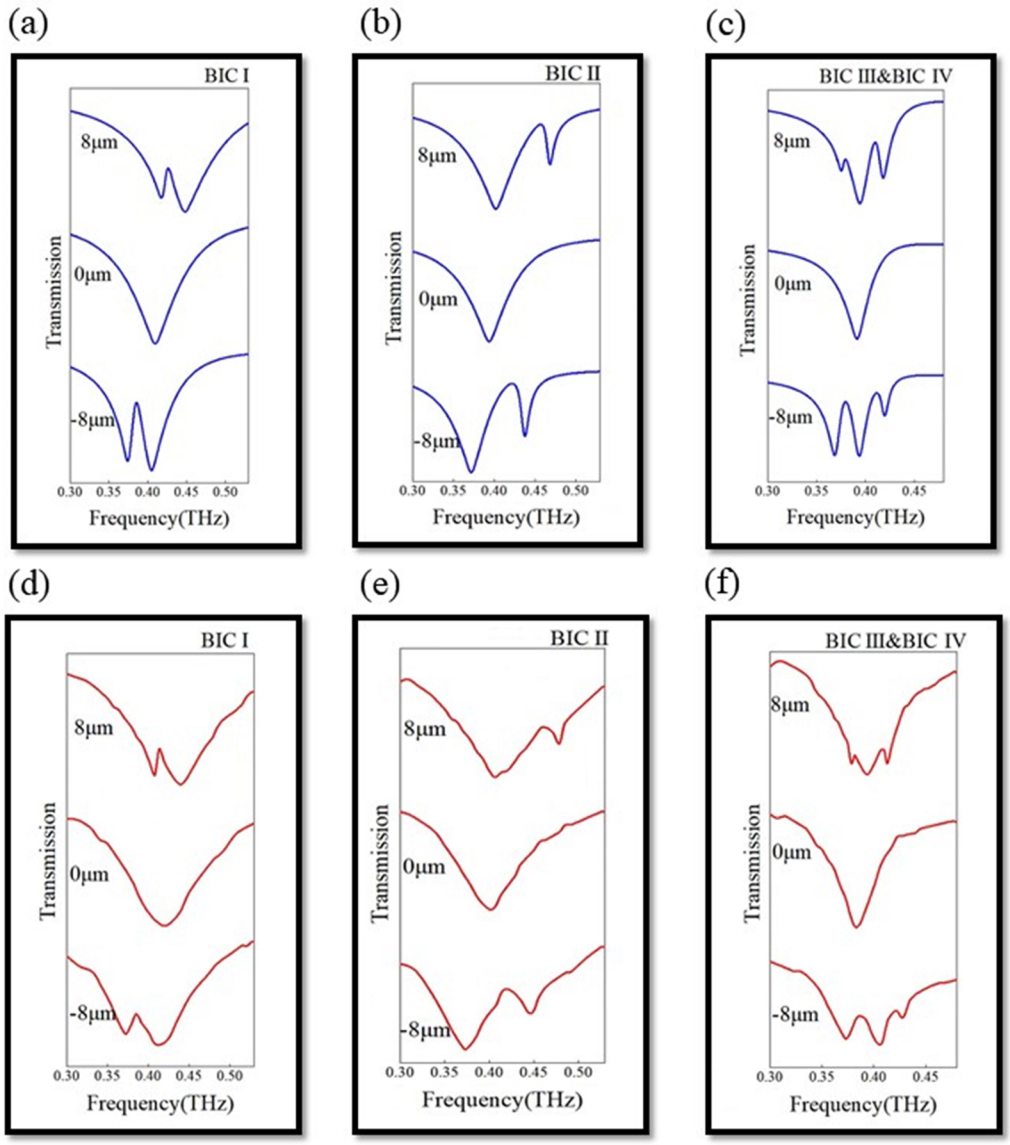

FIG. 6. (a)–(c): Simulated transmission spectra of BIC I, BIC II, and BIC III (BIC IV) in sequence. (d)–(f): The experimentally measured transmission spectra of BIC I, BIC II, and BIC III (BIC IV) in sequence.

Downloaded from http://pubs.aip.org/aip/apm/article-pdf/doi/10.1063/5.0147843/17167793/051102_1_5.0147843.pdf

© Author(s) 2023

III. EXPERIMENT

To experimentally verify the above-mentioned numerical results and the existence of the proposed BIC, we prepared SRR-based BIC and QBIC samples using copper on silicon wafers with a gap width of δ = 8, 0 μm (BIC), and −8 μm. Other dimensions of the SRRs are shown in Fig. 1(a). The thickness of the silicon wafer is 500 μm, and the thickness of the deposited copper is 200 nm. The total size of the as-prepared samples is 9 × 9 mm^2, and Fig. 5(c) shows the microscopic images of the three BIC structures. In this paper, the TDS-1008 THz time-domain spectroscopy system is used to measure the transmission spectrum of the sample, as shown in Fig. 5(a), the working principle diagram of this measurement system.

The system consists of a transmitter, a receiver, and two identical THz focusing lenses. When the THz wave propagates in the air, dry nitrogen gas is continuously injected to remove the water vapor. The sample is placed between the two lenses. A measured time-domain signal is transmitted through the model, and the corresponding air reference signal is shown in Fig. 5(b). The amplitude of the reference signal is larger than that of the sample resulting from the reflection and absorption induced by the sample. In addition, the reference signal is at 50 ps in front of the model, mainly due to the optical length difference caused by attaching eleven 500 μm thick high-resistance silicon substrates close behind the sample substrate to remove the oscillation. The amplitude spectra of the sample and reference samples are obtained through the Fourier transform of the time-domain signal. Through the transmission amplitude spectrum ratio of the loaded signal and the air signal, we can get the transmittance of the sample for the THz wave. The measured time domain length can be up to 140 ps, corresponding to a frequency domain resolution of 7 GHz, which can meet the measurement requirements for the broad QBIC resonance.

To be consistent with the materials used in the experiment, the material PEC of the structure is changed to copper in the CST Microwave Studio, and the frequency domain solver is used to simulate the three superlattices. The numerical simulation calculated the transmission spectrum shown in Figs. 6(a)–6(c). The transmission spectrum results obtained by experimental measurement are shown in Figs. 6(d)–6(f). It can be seen that the measured transmission spectrum is consistent with the results of the numerical simulation, except for some slight differences in details due to experimental errors such as the purity of the metallic copper silicon wafers, the polarization of the sample with respect to the THz signal, etc. When δ = 0 μm, the transmission spectra are the same for all SRRs, and there is only LC resonance with broad line widths in the measured transmission spectra. When the gap between adjacent SRRs in the sample is different, the LC resonance hardly changes, while the QBIC resonance with a narrow linewidth can be observed at the lower (δ = −8 μm) and higher (δ = 8 μm) sides of the BIC frequency. The evolution of BIC to QBIC in three different samples verifies the existence of BIC in the as-prepared metasurface samples. These structurally symmetric-protected BICs are SRRs based on simple LC resonance, which not only provides a clear physical principle for the subsequent research on symmetric-protected BICs but also provides a relatively simple platform for the design of THz devices based on BIC or QBIC. In summary, the evolution of BIC-to-QBIC in the three samples measured experimentally is consistent with the phenomenon of numerical simulation, which verifies the existence of different BICs in the metasurface samples.

IV. CONCLUSION

This paper uses the classical SRR structure to construct the THz BIC metasurfaces. When these metasurfaces break the symmetry in the design, the BIC will transform into a QBIC, and the Q value of the QBIC decreases with the increase in the asymmetry of the system. In summary, we demonstrated multiple BICs/QBICs in a THz metasurface composed of SRRs. These bound states are caused by interference cancellation between neighboring structures. Numerical simulation and experimental results show a complete BIC-to-QBIC evolution process, which confirms the existence of BICs. We prove through experiments that BIC or even double BIC can be produced under different permutation and combination modes by introducing more SRR structures rather than being limited to a single structure. The research results open up a new way for the design of THz devices with high-quality factors that can be effectively implemented.

ACKNOWLEDGMENTS

This work was supported by the National Natural Science Foundation of China (Grant Nos. 61927813 and 61865009).

AUTHOR DECLARATIONS

Conflict of Interest

The authors have no conflicts to disclose.

Author Contributions

T.Z. and X.Z. contributed equally to this work.

Tailin Zhang: Validation (equal); Visualization (equal); Writing – original draft (equal). **Xingyuan Zhang**: Methodology (equal); Visualization (equal); Writing – original draft (equal). **Yun Shen**: Funding acquisition (equal); Resources (equal); Writing – review & editing (equal). **Yinsheng Xu**: Visualization (equal). **Laibin Luo**: Visualization (equal). **Jianqiang Gu**: Resources (equal); Writing – review & editing (equal). **Sijia Yang**: Investigation (equal). **Jie Xu**: Investigation (equal). **Xiaohua Deng**: Funding acquisition (equal).

DATA AVAILABILITY

The data that support the findings of this study are available from the corresponding author upon reasonable request.

REFERENCES

[1] M. Fujita, S. Takahashi, Y. Tanaka, T. Asano, and S. Noda, "Simultaneous inhibition and redistribution of spontaneous light emission in photonic crystals," Science **308**, 1296–1298 (2005).

[2] C. Zhang, T. Xue, J. Zhang, Z. Li, L. Liu, J. Xie, J. Yao, G. Wang, X. Ye, and W. Zhu, "Terahertz meta-biosensor based on high-*Q* electrical resonance

Downloaded from http://pubs.aip.org/aip/apm/article-pdf/doi/10.1063/5.0147843/17167793/051102_1_5.0147843.pdf

© Author(s) 2023

enhanced by the interference of toroidal dipole," Biosens. Bioelectron. **214**, 114493 (2022).
[3]M. S. Luchansky and R. C. Bailey, "High-*Q* optical sensors for chemical and biological analysis," Anal. Chem. **84**, 793–821 (2012).
[4]Y. Yang, W. Wang, A. Boulesbaa, I. I. Kravchenko, D. P. Briggs, A. Puretzky, D. Geohegan, and J. Valentine, "Nonlinear Fano-resonant dielectric metasurfaces," Nano Lett. **15**, 7388–7393 (2015).
[5]C. Jansen, I. A. I. Al-Naib, N. Born, and M. Koch, "Terahertz metasurfaces with high Q-factors," Appl. Phys. Lett. **98**, 051109 (2011).
[6]A. Ferraro, D. C. Zografopoulos, R. Caputo, and R. Beccherelli, "Guided-mode resonant narrowband terahertz filtering by periodic metallic stripe and patch arrays on cyclo-olefin substrates," Sci. Rep. **8**, 17272 (2018).
[7]H. Zhang, W. Zhang, S. Chen, P. Duan, J. Li, L. Shi, J. Zi, and X. Zhang, "Experimental observation of vector bound states in the continuum," Adv. Opt. Mater. (published online, 2023).
[8]W. Koch, "Acoustic resonances in rectangular open cavities," AIAA J. **43**, 2342–2349 (2005).
[9]J. Li, J. Li, C. Zheng, Z. Yue, S. Wang, M. Li, H. Zhao, Y. Zhang, and J. Yao, "Free switch between bound states in the continuum (BIC) and quasi-BIC supported by graphene-metal terahertz metasurfaces," Carbon **182**, 506–515 (2021).
[10]L. Wang, J. Cao, X. Li, Y. Zhao, H. Shi, L. Fu, D. Liu, and F. Liu, "Quasi-BICs enabled proximity sensing based on metal complementary H-shaped arrays at terahertz frequencies," IEEE Photonics J. **14**, 4653608 (2022).
[11]X. Liu, F. Li, Y. Li, T. Tang, Y. Liao, Y. Lu, and Q. Wen, "Terahertz metasurfaces based on bound states in the continuum (BIC) for high-sensitivity refractive index sensing," Optik **261**, 169248 (2022).
[12]M. Kang, L. Mao, S. Zhang, M. Xiao, H. Xu, and C. T. Chan, "Merging bound states in the continuum by harnessing higher-order topological charges," Light-Sci. Appl. **11**, 228 (2022).
[13]A. Tittl, A. Leitis, M. Liu, F. Yesilkoy, D.-Y. Choi, D. N. Neshev, Y. S. Kivshar, and H. Altug, "Imaging-based molecular barcoding with pixelated dielectric metasurfaces," Science **360**, 1105–1109 (2018).
[14]S. I. Azzam and A. V. Kildishev, "Photonic bound states in the continuum: From basics to applications," Adv. Opt. Mater. **9**, 2001469 (2021).
[15]Y. Plotnik, O. Peleg, F. Dreisow, M. Heinrich, S. Nolte, A. Szameit, and M. Segev, "Experimental observation of optical bound states in the continuum," Phys. Rev. Lett. **107**, 183901 (2011).
[16]X. Gao, B. Zhen, M. Soljačić, H. Chen, and C. W. Hsu, "Bound states in the continuum in fiber Bragg gratings," ACS Photonics **6**, 2996–3002 (2019).
[17]M. F. Limonov, M. V. Rybin, A. N. Poddubny, and Y. S. Kivshar, "Fano resonances in photonics," Nat. Photonics **11**, 543–554 (2017).
[18]H. Qin, X. Shi, and H. Ou, "Exceptional points at bound states in the continuum in photonic integrated circuits," Nanophotonic **11**, 4909–4917 (2022).
[19]A. S. Kupriianov, Y. Xu, A. Sayanskiy, V. Dmitriev, Y. S. Kivshar, and V. R. Tuz, "Metasurface engineering through bound states in the continuum," Phys. Rev. Appl. **12**, 014024 (2019).
[20]A. Taghizadeh and I. Chung, "Quasi bound states in the continuum with few unit cells of photonic crystal slab," Appl. Phys. Lett. **111**, 031114 (2017).
[21]Z. Li, Q. Yang, T. Shao, Y. Xu, L. Wang, Q. Xu, X. Zhang, I. Kravchenko, J. Gu, and J. Han, "Terahertz bound state in the continuum in dielectric membrane metasurfaces," New J. Phys. **24**, 53010, (2022).
[22]L. Carletti, K. Koshelev, C. De Angelis, and Y. Kivshar, "Giant nonlinear response at the nanoscale driven by bound states in the continuum," Phys. Rev. Lett. **121**, 033903 (2018).
[23]S. Liu, H. Tong, and K. Fang, "Optomechanical crystal with bound states in the continuum," Nat. Commun. **13**, 3187 (2022).
[24]V. R. Tuz, V. V. Khardikov, A. S. Kupriianov, K. L. Domina, S. Xu, H. Wang, and H.-B. Sun, "High-quality trapped modes in all-dielectric metamaterials," Opt. Express **26**, 2905 (2018).
[25]L. Cong and R. Singh, "Symmetry-protected dual bound states in the continuum in metamaterials," Adv. Opt. Mater. **7**, 1900383 (2019).
[26]S. Campione, S. Liu, L. I. Basilio, L. K. Warne, W. L. Langston, T. S. Luk, J. R. Wendt, J. L. Reno, G. A. Keeler, I. Brener, and M. B. Sinclair, "Broken symmetry dielectric resonators for high quality factor Fano metasurfaces," ACS Photonics **3**, 2362–2367 (2016).
[27]K. Fan, I. V. Shadrivov, and W. J. Padilla, "Dynamic bound states in the continuum," Optica **6**, 169 (2019).
[28]F. H. Stillinger and D. R. Herrick, "Bound states in the continuum," Phys. Rev. A **11**, 446–454 (1975).
[29]X. Zhao, C. Chen, K. Kaj, I. Hammock, Y. Huang, R. D. Averitt, and X. Zhang, "Terahertz investigation of bound states in the continuum of metallic metasurfaces," Optica **7**, 1548 (2020).
[30]X. Zhang, W. Shi, J. Gu, L. Cong, X. Chen, K. Wang, Q. Xu, J. Han, and W. Zhang, "Terahertz metasurface with multiple BICs/QBICs based on a split ring resonator," Opt. Express **30**, 29088–29098 (2022).
[31]M. Tonouchi, "Cutting-edge terahertz technology," Nat. Photonics **1**(2), 97–105 (2007).
[32]A. Y. Pawar, D. D. Sonawane, K. B. Erande, and D. V. Derle, "Terahertz technology and its applications," Drug Invent. Today **5**(2), 157–163 (2013).
[33]M. Hangyo, "Development and future prospects of terahertz technology," Jpn. J. Appl. Phys. **54**(12), 120101 (2015).
[34]R. Singh, W. Cao, I. Al-Naib, L. Cong, W. Withayachumnankul, and W. Zhang, "Ultrasensitive terahertz sensing with high-*Q* Fano resonances in metasurfaces," Appl. Phys. Lett. **105**, 171101 (2014).
[35]B. Reinhard, O. Paul, and M. Rahm, "Metamaterial-based photonic devices for terahertz technology," IEEE J. Sel. Top. Quantum Electron. **19**, 8500912 (2013).
[36]K. Koshelev, S. Lepeshov, M. Liu, A. Bogdanov, and Y. Kivshar, "Asymmetric metasurfaces with high-*Q* resonances governed by bound states in the continuum," Phys. Rev. Lett. **121**, 193903 (2018).
[37]Y. K. Srivastava, M. Manjappa, L. Cong, W. Cao, I. Al-Naib, W. Zhang, and R. Singh, "Ultrahigh-*Q* Fano resonances in terahertz metasurfaces: Strong influence of metallic conductivity at extremely low asymmetry," Adv. Opt. Mater. **4**, 457–463 (2016).
[38]S. Han, L. Cong, Y. K. Srivastava, B. Qiang, M. V. Rybin, A. Kumar, R. Jain, W. X. Lim, V. G. Achanta, S. S. Prabhu, Q. J. Wang, Y. S. Kivshar, and R. Singh, "All-dielectric active terahertz photonics driven by bound states in the continuum," Adv. Mater. **31**, 1901921 (2019).

Downloaded from http://pubs.aip.org/aip/apm/article-pdf/doi/10.1063/5.0147843/17167793/051102_1_5.0147843.pdf

© Author(s) 2023